Metasurfaces with Fano resonances for directionally selective thermal emission

Enas Sakr[1], Deanna Dimonte[1] and Peter Bermel[1,2]

[1]School of Electrical and Computer Engineering, 505 Northwestern Ave., Purdue University, West Lafayette, IN 47907, U.S.A.
[2]Birck Nanotechnology Center, 1205 West State Street, Purdue University, West Lafayette, IN 47907, U.S.A.

ABSTRACT

Thermal emission impacts a wide variety of applications, including thermophotovoltaics, photovoltaics, photon-enhanced thermionic emission, selective solar absorption, incandescent lighting, and spectroscopy. Ordinary structures generally emit a broad range of wavelengths, angles, and polarizations. However, highly selective thermal emission has potential to greatly improve performance in many of these applications. While prior work has explored a wide range of structures to provide some degree of control of one or more of these attributes, there is an ongoing challenge in combining readily-fabricated, simple structures made of appropriate (e.g., heat-resistant) materials with the desired functionality. Here, we will focus on using metasurfaces in conjunction with refractory materials as a platform for achieving selective control of emission. These structures are built from sub-wavelength elements that support localization of surface plasmon polaritons or electromagnetic resonant modes with appropriate attributes. Modeling is performed using rigorous coupled wave analysis (RCWA), plus Kirchhoff's law of thermal radiation, which is further validated using finite-difference time domain (FDTD) simulations and coupled-mode analysis. Such structures can be considered arbitrarily directional sources that can be carefully patterned in lateral directions to yield a thermal lens with a designed focal length and/or concentration ratio; the benefit of this approach is that it can enhance the view factor between thermal emitters and receivers, without restricting the area ratio or separation distance. This design and modeling platform is then applied to exclude thermal radiation over a certain range of angles. In this work, we study the effect of controlling the angular width and direction on the view factor, and we explore angular dependence of these angular selective structures.

INTRODUCTION

Thermophotovoltaics is a direct method to convert heat into electricity. Typically, the thermal-to-electricity conversion process involves a thermal emitter, heated up by a thermal source, which could come from hydrocarbon fuel, radioisotope decay, or solar energy [1], to temperatures as high as 1700 K. The thermal emitter radiates electromagnetic energy in forms of thermal photons towards a photovoltaic cell. Only thermal photons with energies higher than the bandgap of the photovoltaic (PV) cell will contribute to the photocurrent generation. The absorbed photons separate electron hole pairs which are then conducted to electrodes and collected as output electric power. Filters can also be placed between the emitter and the converter to reduce parasitic losses, and recycle low energy photons that are not absorbed by the PV cell. Cold side filters include plasma filters [2,3], quarter wave stacks [4], or rugate filters [5,6]. Integrated filters in the emitter's side are also suggested to enhance efficiency by reducing parasitic losses [7,8]. Fig. 1(a) demonstrates the TPV conversion process.

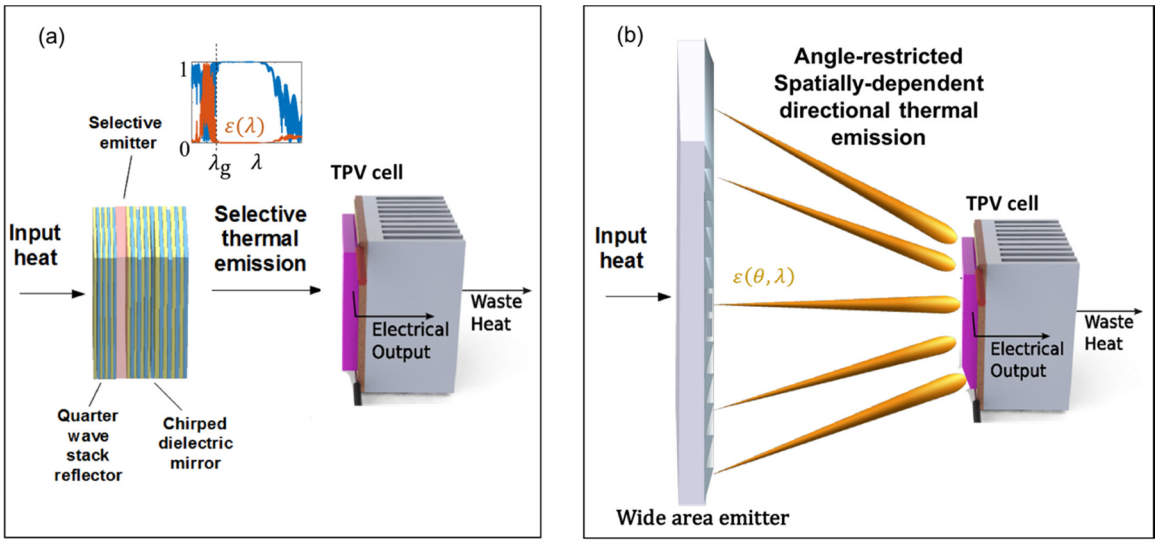

Fig.1 (a) In thermophotovoltaic conversion of heat to electricity, a wavelength-selective emitter with a spectrum matched to the PV device bandgap enhances efficiencies. (b) An angle-selective emitter placed away from the PV device efficiently directs thermal emission to a distant receiver.

To maintain a high view factor, emitters are typically placed close to the PV converter, this in turn requires effective cooling techniques for PV diodes. In this work, a new strategy is suggested to improve the view factor between a planar emitter and receiver, with relaxed restrictions on the separation distance between them and their area ratio. The proposed design makes use of angle-restricted, directional thermal emitters with arbitrary directionality [9]. These directional elements can be arranged and engineered over the emitter surface to focus all the emission on the receiver, as shown in Fig. 1(b). This technique was previously suggested for achromatic metasurfaces [10], and focusing of surface plasmon polariton (SPP) modes [11].

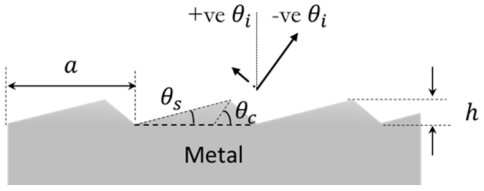

Fig.2 A metallic periodic blazed grating for symmetric-sensitive emission. The period a, and the angles θ_s, θ_c, and the height h control the direction of emission and the maximum emissivity amplitude at a given wavelength.

The directional elements are periodic metallic gratings with asymmetric geometry that couples thermally excited SPP modes to free space propagating modes. Potential directional emitters are lamellar gratings [12,13], sawtooth or blazed gratings [9,11], and slanted gratings [14]. An example of symmetric-sensitive directional grating is shown in Fig. 2. The asymmetric angle-dependent emission was discussed in a previous work [9].

Finally, we consider how Fano resonances can be used to create a complementary pattern *excluding* thermal emission over a narrow angular range. These structures may also have their own set of applications and/or in combination with narrow angular range emitters.

THEORY

To estimate the improvement of the transfer of power from a source to a receiver based on directional thermal emitters, as shown in Fig. 1b, it is useful to quantify the limits of the fraction of emitted power that can be received (the view factor) in the ideal case of angle-restricted elements of angular width $\Delta\theta$ emitting with unit emissivity in an arbitrary direction θ, as a function of various length ratios and separation distances between the emitter and the receiver, and assuming zero emissivity otherwise.

In two dimensions, the view factor between an infinite stripe of width l_1, facing, and parallel to an infinite stripe of width l_2, with a separation distance d between them is defined by the following relation, as derived from [15]:

$$F_{12} = \lim_{w_1,w_2\to\infty} \frac{1}{l_1 w_1} \frac{\iint_{y_1=-w_1/2,x_1=-l_1/2}^{y_1=w_1/2,x_1=l_1/2} d\,x_1 dy_1 \iint_{y_2=-w_2/2,\,x_2=-l_2/2}^{y_2=w_2/2,\,x_2=l_2/2} d\,x_2 dy_2 \frac{\cos^2\theta}{\pi r^2}}{\iint_{y_1=-w_1/2,x_1=-l_1/2}^{y_1=w_1/2,x_1=l_1/2} d\,x_1 dy_1 \iint_{y_2=-w_2/2,\,x_2=-\infty}^{y_2=w_2/2,\,x_2=\infty} d\,x_2 dy_2 \frac{\cos^2\theta}{\pi r^2}}, \quad (1)$$

where $r = \sqrt{(x_2 - x_1)^2 + (y_2 - y_1)^2 + d^2}$, and $\cos\theta = d/r$. The above equation first computes the radiated power from an infinitesimal area $d\,x_1 dy_1$ on the surface of the emitter that is intercepted by the receiver, then is integrated over the surface area of the emitter, and finally divided by the total emitted power by the emitter in space.

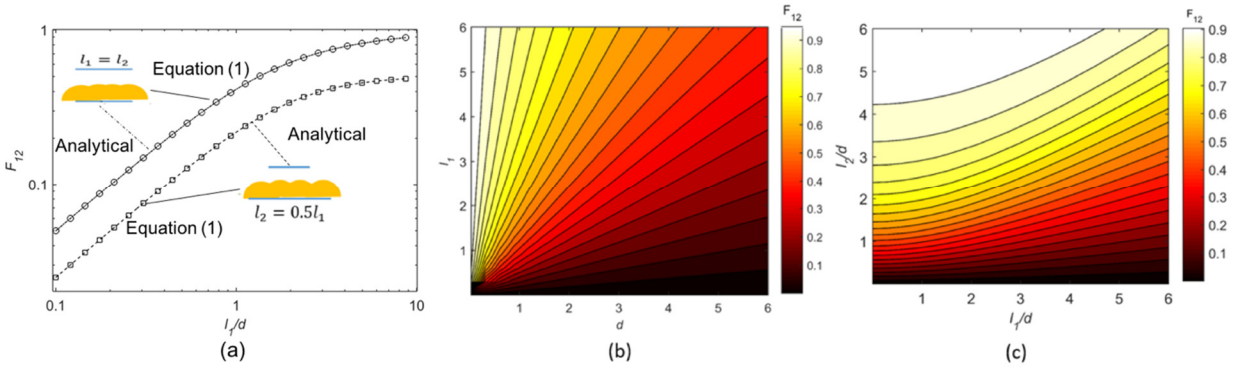

Fig. 3 (a) View factor in 2D between parallel stripes of the same widths (circles) and of unequal widths (squares) computed using (1), and with excellent matching to the analytical solution from [15] (dash-dotted and dashed, respectively). (b) The view factor of equal plates of widths l_1 separated by distance d. A unity view factor is obtained when $d \ll l_1$. (c) The view factor between two stripes of unequal widths. A unity view factor is observed when $l_1 < l_2$, photon recycling losses are not taken into account in this computation.

First, we validate this approach by confirming that the results obtained from (1) for $l_1 = l_2$ and $l_2 = 0.5l_1$ and plotted in Fig. 3(a), match very well with the analytical solution obtained in prior work [15]. Then a contour plot of the unrestricted view factor is computed for the case when $l_1 = l_2$ with different values of separation distance, and plotted in Fig. 3(b). The plot implies that a unity view factor is not possible, unless the two stripes are closely separated. Finally, a contour plot of the view factor with different values of l_1 and l_2 at a fixed distance d is plotted in Fig. 3(c). The plot implies that a unity view factor is achieved, if $l_1 < l_2$, or simply when all the emitted power is collected by the wide receiver. Although this is a simple solution to increase the view

factor, it does not take into account the photon recycling effect. If the photon recycling is taken into account, losses in the view factor will arise because of the portion of emitted power that is not reflected back towards the emitter. Consequently, the proposed design in Fig. 1(b) is advantageous for external photon recycling.

RESULTS & DISCUSSION

View factor enhancement

In the following, we place *ideal* directional, angle-restricted emitters on the emitter surface, with the directional angle designed to change linearly over the surface, to be directed towards the emitter. We first consider the case when the two stripes have the same width $l_1 = l_2 = L$. In this case, all the directional elements are emitting towards the normal direction. Fig. 4(a) shows the view factor for separation distances ranging from $d = 0$ to $d = 5L$, and with angular widths $0 < \Delta\theta < 180°$. The view factor reaches unity for very small values of $\Delta\theta \sim 1°$, or for very small values of d, and degrades quickly, especially for larger separation distances. This strict angular dependence makes the design vulnerable to any background non-directional emission, since the portion of the directional power to the total power is small. Hence, with more realistic lossy directional emitters, a close-to-unity view factor is very difficult to maintain in this situation.

The second case is shown in Fig. 4(b), where the directional angle is allowed to conform with from the edge of the emitter to the edge of the receiver, and decreases linearly till it reaches zero at the centers. Assuming that the emitter's width is 5 times the receiver's width, the view factor is plotted in Fig. 4(b). It is evident that a close-to unity view factor is possible for highly restricted angular emitters, i.e. $\Delta\theta \sim 1°$. However, the view factor also degrades quickly for larger values of $\Delta\theta$, especially for larger separation distances.

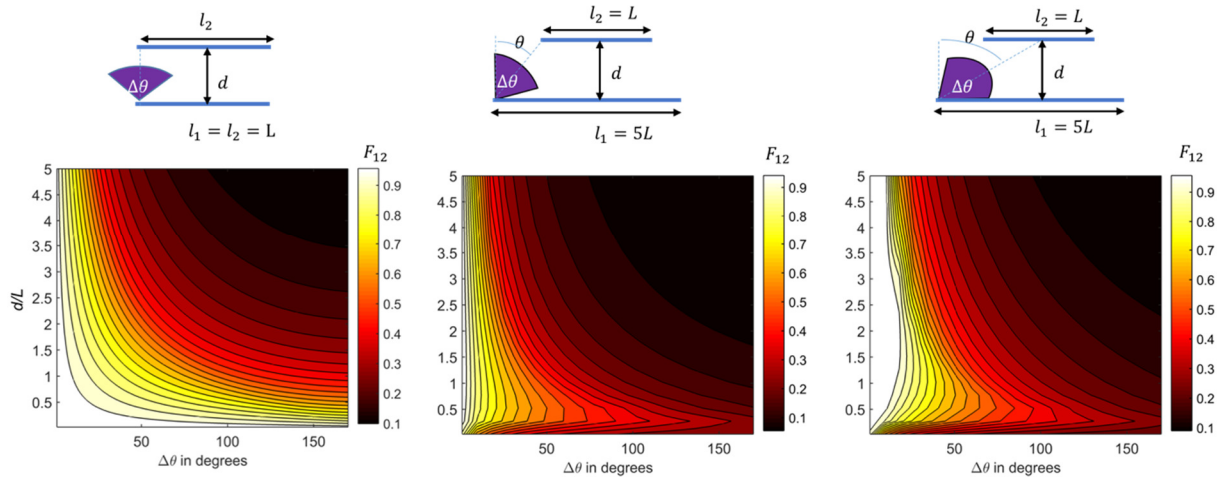

Fig. 4 View factor between emitter and receiver with engineered restricted-angle directional emitters. (a) Two stripes of similar widths. (b) Emitter larger than the receiver with edge-to-edge engineered directional emission. (c) Same as (b) but with concentrated engineered directional emission. The view factor in (c) remains near unity for a wide range of restricted angles that make this design more immune to losses.

Thus an improved design that relaxes this strict condition is to arrange the directional angles to target the center of the receiver, as shown in Fig. 4(c). The corresponding view factor equals unity for values of $\Delta\theta < 10°$, thus it is expected to design practical directional emitters with small

background non-directional emission. This situation suggests that the required directional emitters should exhibit sufficiently low integrated background emitted power, compared to the portion of emitted power directed towards the receiver. In fact, this condition might be satisfied for low loss metals, such as Tantalum, at long wavelengths, e.g. at 2500 nm. The only problem in this case, is that the angular width, and the maximum directional emissivity both depend on the absorption loss quality factor of the material, hence the directional peak will have small angular widths < 1°. However, it is possible that a finite number of periods of gratings [16] would exhibit an increased angular width, as a result of applying a spatial window function to the periodic grating structure, similar to the array factor of antenna arrays [13].

As a next step, it is appropriate to test the performance of symmetric-sensitive designed emitters, for example similar to the sawtooth or blazed grating designed in reference [9], and shown in Fig. 2, by placing them with their emissivity function in the view factor computation, and hence estimate the losses that arise from the off-directional emission. It is expected, as mentioned before, that the design in Fig. 4(c) should show higher view factor than the configurations in Fig. 4(a) and Fig. 4(b).

To simulate these more realistic structures and see how close they come to the ideal case, we have several options, including the finite difference time domain FDTD method [18], the transfer (T-) and scattering (S-) matrix methods [19], and the Fourier modal method (FMM) or the rigorous coupled wave analysis (RCWA) [20,21]. The selection of the simulation method depends on the specific design of the structures and materials. For example, the RCWA method is useful for simulating periodic 2D structures, the S- and T-matrix approaches are useful to study multilayer structures, while FDTD method can solve arbitrary, periodic or non-periodic 1D, 2D, or 3D structures. A useful frequency domain open source code developed by Liu and Fan is the Stanford Stratified Structure Solver (S4) [21], which combines the S-matrix approach with the RCWA method. Since all the structures investigated in this work are either multi-layer structures or periodic gratings, S4 is used to solve for the emissivity as a function of wavelength and incident angle. Another useful FDTD open source code developed in MIT is MEEP [22], which will also be used for resonant modes extraction and obtaining absorptivity spectra. In the following section, we use a combination of MEEP and coupled mode theory to validate our understanding of these angular emitters.

Coupled mode theory analysis of Fano resonance directional modes

The directional absorption by metallic grating exhibits an asymmetric Fano-resonant shape, as a result of the interference between the bulk metallic absorption background, and the resonant SPP absorption. In this way, the emission spectra obtained for metallic gratings, can be analyzed in the framework of the coupled mode theory (CMT) [23]. Hence, it is possible to obtain the optimum dimensions of the grating, as well as the optical constants of the metal, that will enhance emissivity at the target wavelength and angle, without the need to invoke exhaustive absorption simulation with optimization algorithm. The main concept depends on satisfying the Q-matching condition [24]. The Q-matching condition is directly obtained from the CMT for resonant modes with quality factors larger than 20. Hence the absorption is maximized when the absorption loss rate equals the radiation loss rate, as a result of impedance matching between the two loss rates. Then, by Kirchhoff's law of thermal radiation, the emissivity is maximized as well.

A useful tool for obtaining the resonant modes and their quality factors (Q) is the harmonic inversion (Harminv) [25] function implemented in MEEP [22], which expresses the resonant modes into a summation of complex harmonics, and then extracts the resonant modes and their quality factors. Applying Harminv on the lamellar grating case, designed in reference [12], showed a good agreement with the obtained resonant peak from absorption simulation, as shown in Fig. 5. The lamellar grating is made of Tungsten at 4530 nm with period $a = 0.66225\lambda$, and depth $t = 0.02759\lambda$, and 50% duty cycle. The lamellar grating structure is depicted in the inset of Fig. 5.

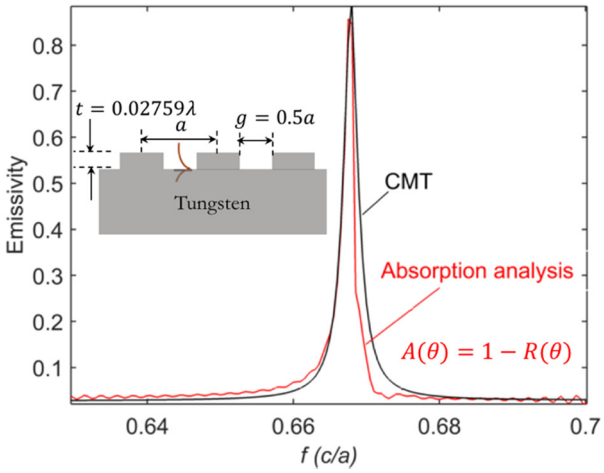

Fig.5 The directional resonant peak obtained from CMT (solid) in good agreement with the absorption simulation (dashed). The lamellar grating structure is shown in the inset.

The radiation quality factors are obtained by removing the losses from the metal and obtaining the resonant modes by Harminv. The losses then are inserted again to obtain the total quality factors, from which the absorption quality factors can be extracted. For the studied lamellar grating case, two modes where found at frequencies of 0.6679 and 0.668 in meep units, and total Q of 294, 783, respectively, and radiative Q of 469, 1969, respectively. It is thus expected that applying the coupled mode theory can easily describe the resonant spectrum of different grating geometries, hence assists in designing their parameters based on the Q-matching condition [26,27].

Finally, preliminary studies of the effects of these types of emitters have shown the dominant role that parasitic emission can play in the case of high-Q emitters. While tungsten in the near-infrared may not be sufficient to achieve a large enhancement of the power transfer because of this loss mechanism, adding filters or operating at longer infrared wavelengths may be a regime where significant advantages to this approach can be realized.

Normal angular absorption prohibition

Now we consider the complementary emitter scenario, where the radiating element is required to exhibit emission in all directions, except for a specific range of angles, where the emission should be prohibited. Some applications may require this sort of behavior, such as the protection of vulnerable elements from direct exposure to heat radiation. This kind of device can be realized utilizing an angular selective transmission filter, placed on top of a radiating/absorbing element. The proposed structure makes use of a high contrast grating (HCG) [28], or a high-index dielectric photonic crystal slab [24], that show wideband reflectivity for normal incidence, and slightly off-normal incidence [29]. The wideband reflection is attributed to destructive interference of spatial modes at the exit of the gratings [28]. However, for higher values of lateral momentum or k_x, Fano-resonant transmission modes are coupled. It was shown that the HCG does not keep the wideband reflectivity property for all the incident angles, except for a narrowband of angular range around zero [29], beyond which coupling to narrowband

transmission mode takes place. Hence, it is expected that absorption (or emission by Kirchhoff's law) in or from the absorbing substrate is reflected by the HCG for a narrow angular range around the normal incident angle at the resonance frequency. The proposed structure is depicted in Fig. 6(a).

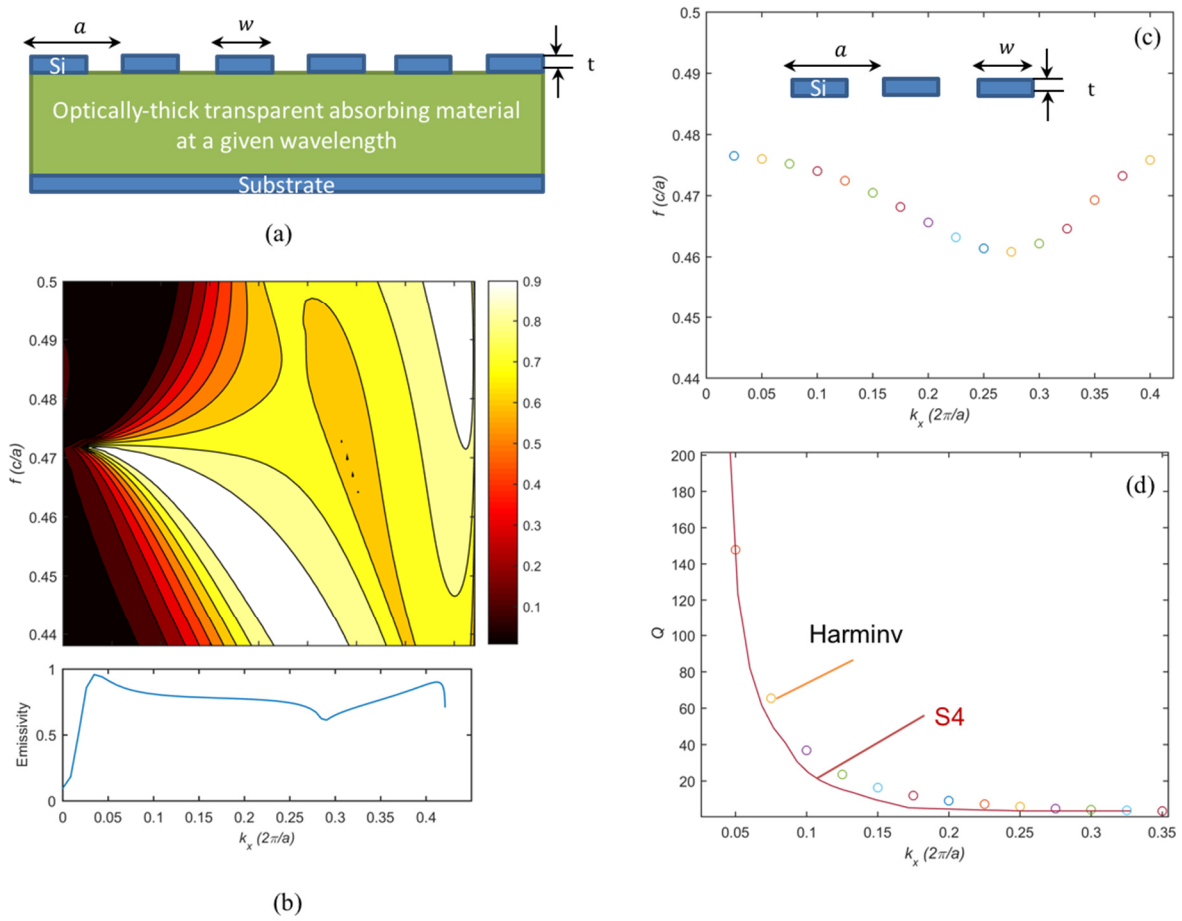

Fig. 6 (a) The structure suggested for forbidden absorption around the normal direction: resonant HCG on the absorbing material on a substrate. (b) Contour plot of the directional absorption, the bottom panel is the directional absorption with a dip around normal, measured at *f=0.47 (c/a)*. (c) The bandstructure of the resonant grating in air, in good agreement with the resonant band in (b). (d) The quality factor obtained from MEEP and from absorption simulation in S4 as extracted from (b).

A preliminary design uses a Si grating, assuming that it is thermally transparent at the wavelength of interest. The period a of the grating is kept at 700 nm, with a Si width w of $0.77a$, and thickness (t) of 400 nm. The dielectric constant of the absorber is 2.5+0.005i, and is assumed to be optically-thick to obtain the maximum absorption. It is worth mentioning that the absorber material is not required to exhibit strong absorption coefficient, since the grating filter controls the transmission to the absorbing substrate. Hence, the only requirement is to maintain an optically-thick absorber substrate. The emissivity is calculated using S4 and plotted for different values of wavelengths from 1400 nm to 1500 nm and incident angles from 0 to 87°. The bandstructure of the Si grating suspended in air is also computed using harmonic inversion

function (Harminv) [25] in MEEP [22]. Fig. 6(c) shows the computed bandstructure for p-polarized modes for different values of the lattice vector k_x. For the sake of comparison, the calculated emissivity from S4 is plotted in Fig. 6(b), with normalized frequency and wavevector units of (c/a), and $(2\pi/a)$, respectively, comparable to MEEP units. The bottom panel of Fig. 6(c) shows the stop-angle filtering behavior of the device at $f = 0.4717c/a$. In comparison with the bandstructure in Fig. 6(a), the obtained band is shifted by a slight amount, but the quality factors extracted from the resonant modes in Fig. 6(b) and Fig. 6(c) are in reasonable agreement. The quality factor of the Fano-resonant mode extracted from the emissivity calculation is measured as the nearest frequency to the frequency of maximum amplitude that has an amplitude half of that of the peak amplitude.

Since Si shows an increased free-carrier absorption at near infrared wavelengths, it could potentially be replaced by a low-absorbing high bandgap material, such as GaN, AlN, or SiC. In this case, the dimensions of the grating then should be optimized to maintain a similar bandstructure and reflectivity at the wavelength of interest. Of course, the greatest benefit of this approach would be achieved with arbitrary direction tuning, unless the emitter is assumed to be much smaller than the receiver.

CONCLUSIONS

In conclusion, we found that angular restriction has potential to significantly enhance thermal transfer between a source and a receiver, particularly if the angular restriction can be continuously graded to point toward the center of the receiver plane. We then discussed Fano resonances as a particular approach capable of both creating narrowband emission at targeted frequencies and angles. We first showed good agreement between the performance predicted by FDTD simulations and coupled mode theory. We then considered the potential for emitting over many angles except close to the normal, and showed that FDTD and RCWA simulation techniques match fairly well. In future work, we will consider whether introduction of volume plasmonic polariton modes are capable of providing a broader range of angles with less frequency dispersion, as might be predicted from the plasmonic dispersion line.

ACKNOWLEDGMENTS

Support was provided by the Department of Energy, under DOE Cooperative Agreement No. DEEE0004946 (PVMI Bay Area PV Consortium), the NEC Corporation, Northrop Grumman Aerospace Systems in support of “Ultra-thin metasurfaces for redirecting light and managing thermal emission,” and the NSF Award EEC 1454315 - CAREER: Thermophotonics for Efficient Harvesting of Waste Heat as Electricity.

REFERENCES

1. T. Bauer, *Thermophotovoltaics: Basic Principles and Critical Aspects of System Design*, Green Energy and Technology (Springer, 2011).
2. O. Vigil, C. M. Ruiz, D. Seuret, V. Bermúdez, and E. Diéguez, "Transparent conducting oxides as selective filters in thermophotovoltaic devices," J. Phys. Condens. Matter **17**, 6377–6384 (2005).
3. Z. G. Qian, W. Z. Shen, H. Ogawa, and Q. X. Guo, "Infrared reflection characteristics in InN thin films grown by magnetron sputtering for the application of plasma filters," J. Appl. Phys. **92**, 3683 (2002).
4. F. O'Sullivan, I. Celanovic, N. Jovanovic, J. Kassakian, S. Akiyama, and K. Wada, "Optical characteristics of one-dimensional Si/SiO2 photonic crystals for thermophotovoltaic applications," J. Appl. Phys. **97**, 033529 (2005).
5. C. K. Carniglia, "Comparison of several shortwave pass filter designs," Appl. Opt. **28**, 2820–3 (1989).
6. U. Ortabasi, "Rugate Technology For Thermophotovoltaic (TPV) Applications: A New Approach To Near Perfect Filter Performance," in *Fifth Conference on Thermophotovoltaic Generation of Electricity* (AIP Publishing, 2003), Vol. 653, pp. 249–258.
7. E. S. Sakr, Z. Zhou, and P. Bermel, "High efficiency rare-earth emitter for thermophotovoltaic applications," Appl. Phys. Lett. **105**, 111107 (2014).
8. Z. Zhou, O. Yehia, and P. Bermel, "Integrated photonic crystal selective emitter for thermophotovoltaics," J. Nanophotonics **10**, 016014 (2016).
9. E. Sakr, S. Dhaka, and P. Bermel, "Asymmetric angular-selective thermal emission," in *Proc. SPIE 9743, Physics, Simulation, and Photonic Engineering of Photovoltaic Devices V* (2016), Vol. 9743, p. 97431D.
10. F. Aieta, M. A. Kats, P. Genevet, and F. Capasso, "Multiwavelength achromatic metasurfaces by dispersive phase compensation," Science (80-.). **347**, 1342–1345 (2015).
11. M. S. Kumar, X. Piao, S. Koo, S. Yu, and N. Park, "Out of plane mode conversion and manipulation of Surface Plasmon Polariton Waves," Opt. Express **18**, 8800 (2010).
12. M. Laroche, C. Arnold, F. Marquier, R. Carminati, J.-J. Greffet, S. Collin, N. Bardou, and J.-L. Pelouard, "Highly directional radiation generated by a tungsten thermal source," Opt. Lett. **30**, 2623 (2005).
13. J.-J. Greffet, R. Carminati, K. Joulain, J.-P. Mulet, S. Mainguy, and Y. Chen, "Coherent emission of light by thermal sources.," Nature **416**, 61–4 (2002).
14. N. Bonod, E. Popov, L. Li, and B. Chernov, "Unidirectional excitation of surface plasmons by slanted gratings," Opt. Express **15**, 11427 (2007).
15. M. F. Modest, *Radiative Heat Transfer* (Academic Press, 2013).
16. K. Hirayama, E. N. Glytsis, and T. K. Gaylord, "Rigorous electromagnetic analysis of diffraction by finite-number-of-periods gratings," J. Opt. Soc. Am. A **14**, 907 (1997).
17. C. A. Balanis, *Antenna Theory: Analysis and Design* (John Wiley & Sons, 2016).
18. A. Taflove and S. C. Hagness, *Computational Electrodynamics: The Finite-Difference Time-Domain Method* (Artech House, 2000).
19. D. M. Whittaker and I. S. Culshaw, "Scattering-matrix treatment of patterned multilayer photonic structures," Phys. Rev. B **60**, 2610–2618 (1999).
20. M. G. Moharam and T. K. Gaylord, "Rigorous coupled-wave analysis of planar-grating

diffraction," J. Opt. Soc. Am. **71**, 811 (1981).
21. V. Liu and S. Fan, "S4 : A free electromagnetic solver for layered periodic structures," Comput. Phys. Commun. **183**, 2233–2244 (2012).
22. A. F. Oskooi, D. Roundy, M. Ibanescu, P. Bermel, J. D. Joannopoulos, and S. G. Johnson, "Meep: A flexible free-software package for electromagnetic simulations by the FDTD method," Comput. Phys. Commun. **181**, 687–702 (2010).
23. W. Suh, Z. Wang, and S. Fan, "Temporal coupled-mode theory and the presence of non-orthogonal modes in lossless multimode cavities," IEEE J. Quantum Electron. **40**, 1511–1518 (2004).
24. D. L. C. Chan, I. Celanovic, J. D. Joannopoulos, and M. Soljačić, "Emulating one-dimensional resonant Q -matching behavior in a two-dimensional system via Fano resonances," Phys. Rev. A - At. Mol. Opt. Phys. **74**, 1–4 (2006).
25. V. A. Mandelshtam and H. S. Taylor, "Harmonic inversion of time signals and its applications," J. Chem. Phys. **107**, 6756–6769 (1997).
26. R. Shugayev and P. Bermel, "Time-domain simulations of nonlinear interaction in microring resonators using finite-difference and coupled mode techniques.," Opt. Express **22**, 19204–18 (2014).
27. J. D. Joannopoulos, S. G. Johnson, J. N. Winn, and R. D. Meade, *Photonic Crystals: Molding the Flow of Light*, 2nd ed. (Princeton, 2008).
28. V. Karagodsky, F. G. Sedgwick, and C. J. Chang-Hasnain, "Theoretical analysis of subwavelength high contrast grating reflectors.," Opt. Express **18**, 16973–16988 (2010).
29. J. M. Foley, S. M. Young, and J. D. Phillips, "Narrowband mid-infrared transmission filtering of a single layer dielectric grating," Appl. Phys. Lett. **103**, (2013).